PHOTONICS Research

Disclosing transverse spin angular momentum of surface plasmon polaritons through independent spatiotemporal imaging of its in-plane and out-of-plane electric field components

Yulu Qin,[1] Boyu Ji,[1] Xiaowei Song,[1,2] and Jingquan Lin[1,*]

[1]Department of Physics, Changchun University of Science and Technology, Changchun 130022, China
[2]e-mail: songxiaowei@cust.edu.cn
*Corresponding author: linjingquan@cust.edu.cn

Received 13 November 2019; revised 28 December 2019; accepted 14 April 2020; posted 16 April 2020 (Doc. ID 382426); published 1 June 2020

The comprehensive capture of near-field spatiotemporal information of surface plasmon polaritons (SPPs) is a prerequisite for revealing their physical nature. In this study, we first performed an independent, spatiotemporal imaging of the out-of-plane and in-plane components of SPP near-fields in a femtosecond light-excited trench using an obliquely incident time-resolved photoemission electron microscopy (TR-PEEM). We did the capture by imaging of the interference patterns induced by a superposition of the *p*- or *s*-polarized probe light, with the out-plane or in-plane components of SPP near-fields, under the noncollinear excitation mode. The method may be used to reconstruct a 3D SPP spatiotemporal field. Moreover, we demonstrated that the fringe shift of the interference patterns between the captured in-plane and out-of-plane components of the SPP field in PEEM images corresponds to the 1/4 fringe period, which is attributed to $\pi/2$ out of phase of the out-of-plane and in-plane near-field components of SPP. The resulting TR-PEEM images are supported by a classical wave mode and FDTD simulations. Essentially, the measured $\pi/2$ phase difference between the in-plane and out-of-plane components of the SPP indicated a rotating field component in the propagation plane, i.e., that the SPP exhibits an elliptically polarized electric field in the propagation plane. The experimental results presented herein provide direct evidence of SPP having the inherent attributes of transverse spin angular momentum.

https://doi.org/10.1364/PRJ.382426

1. INTRODUCTION

The transverse spin angular momentum (TSAM) of a surface plasmon polariton (SPP), being perpendicular to the SPP wave vector, plays a crucial role in various light–matter interactions [1,2]. On the one hand, TSAM matching determines the coupling of excitation light into SPP fields [3], which makes it a viable option in experiments to control the directional launching of SPP [4–6]. On the other hand, TSAM is closely related to the plasmonic Hall effect [4,5]; thus, for the chemical community, the control over spin may enable selective excitation of chiral molecules [5]. Moreover, the TSAM of an SPP field gives rise to lateral optical forces on chiral particles [7], assigning it with potential utilization in engineering optical manipulation, such as for optical tweezers. With this, a significant task for understanding the essence of TSAM and achieving SPP applications is to experimentally reveal the TSAM of an SPP.

Several studies have indirectly confirmed the TSAM in terms of far-field spectroscopy by determining the scattering direction of spin-carrying photons [8] or the numerical simulation by calculating the force and torque acting on a Mie particle in the SPP field [2,7]. However, the far-field spectra carry only limited information about the nature of SPP; further, it is impractical to measure the mechanical properties of Mie particles in the SPP field in experiments. Therefore, they are still some distance away from the essential disclosing of TSAM of the SPP.

A theory has previously identified TSAM of SPP to arise from the imaginary longitudinal electric field, which generates the rotation of the electric field vector within the propagation plane, and this corresponds to the out-of-plane and in-plane electric field components of SPP, which have a phase difference of $\pi/2$ [1,2]. Essentially, it is reliable to mention that the TSAM of SPP can be verified by independently capturing the instantaneous phase information of these out-of-plane and in-plane near-fields, and the probe of transient information of both components is a prerequisite for understanding the

generation and evolution of the TSAM of SPP. Unfortunately, to date, the techniques to probe the spatiotemporal characteristics of SPP, such as scanning near-field optical microscopy (SNOM) [9], leakage-field radiation microscopy [2,10], or nonlinear fluorescence microscopy [11], are all faced with the great challenge to independently capture the spatiotemporal information of the respective components of SPP near-fields, although the static information of the out-of-plane and in-plane components of SPP can be measured by employing SNOM customized complex probes [12,13]. Researchers have recently demonstrated the spatiotemporal imaging of SPP using a time-resolved photoemission electron microscope (TR-PEEM) [14–16] as well as having successfully measured the propagation length [15] and group velocity [15] of SPP, especially its in-plane field components with normally incident TR-PEEM [17–19]. However, because of interference patterns in a normally incident PEEM image from the interference of the incident laser light with the in-plane component of the SPP's electric field [20], dynamic information on the out-of-plane component of the SPP has insurmountably and undoubtedly been missed. To the best of our knowledge, there has been no actual experiments yet conducted for an independent spatiotemporal imaging of the respective components of SPP near-fields.

In this paper, we carry out, initially, such independent spatiotemporal imaging of out-of-plane and in-plane components of the SPP field in the femtosecond light excited trench with obliquely incident TR-PEEM. We captured the components by using *p*- and *s*-polarized femtosecond laser probes of SPP near-field generated under the noncollinear excitation of a trench structure (the in-plane component of the laser wave vector that is noncollinear with the *k*-vector of SPP) and imaging of an interference fringe induced by the superposition of the *p*- or *s*-polarized probe light with the out-of-plane or in-plane components of SPP near-fields. TR-PEEM images obtained by the pump-probe method disclose that the out-of-plane and in-plane near-field components of the same SPP are always $\pi/2$ out of phase, a result supported by a classical wave model calculation and finite-difference-time-domain simulations. The results presented herein provide direct evidence that an SPP exhibits an elliptically polarized electric field in the propagation plane and has a TSAM nature.

2. METHODS

The rectangular 20 μm × 1 μm and 10 μm × 1 μm trench coupling structures are milled into ~100 nm thick silver thin film on a clean Si substrate using a focused ion beam (FIB) lithography. A Ti:sapphire laser oscillator (Coherent, Mira 900), which provides ~130 fs duration pulses at an 800 nm center wavelength with 76 MHz repetition rate, tunable output wavelength in the 680–900 nm range, and frequency doubling in a β-$BaBO_3$ (BBO) crystal, produces tunable excitation pulses in the 360–440 nm band.

A typical work function of silver, depending on the crystal orientation and morphology of nanostructure, is 4.26 eV. Accordingly, the nonlinear order of the photoemission in the experiment for the laser wavelength of 400 nm corresponds to 2 and for 750 nm to 3. Meanwhile, the laser power of 150–400 mW for the wavelength of 750 nm and power of 30–50 mW for the 400 nm were used, respectively, in the experiment. The multiphoton photoemission from a superposition of SPP and laser field are recorded using a photoemission electron microscope (Focus GmbH). The Focus PEEM essentially consists of an imaging electrostatic lens system and an image acquisition device. Typically, the spatial resolution, as defined by edge contrast, is better than 30 nm for a simple electrostatic lens column without aberration correction. The incident laser is focused onto the sample surface using a 20 cm focal length off-axis parabolic mirror at an incident angle of 65° with respect to the surface normal, which is determined by the PEEM instrument; further, under these conditions, elliptically shaped focused laser spots are observed featuring major/minor axes of 70/40 μm. For dual-beam experiments, the pulses are interferometrically locked using a Mach–Zehnder interferometer with each arm having separate polarization control by half-wave plate and control the position of the probe light pulse by adjusting the beam combiner. Details on the experiment setup have been reported in our previous publication [21].

Numerical simulations were performed using a commercial FDTD package (Lumerical FDTD Solutions). The calculations employ a total field-scattered plane wave source that allows monitoring pure instantaneous phase information of out-of-plane and in-plane near-fields of the same SPPs (does not contain incident light electric field). The dielectric permittivity of silver is taken from Johnson and Christy [22].

3. RESULTS AND DISCUSSION

Figures 1(a) and 1(d) display two schematic illustrations of a single-beam PEEM experiment of the collinear mode (the in-plane component of the laser wave vector that is collinear with the SPP *k*-vector) and noncollinear mode excitation (the in-plane component of the laser wave vector that is noncollinear with the SPP *k*-vector). Throughout the paper, to

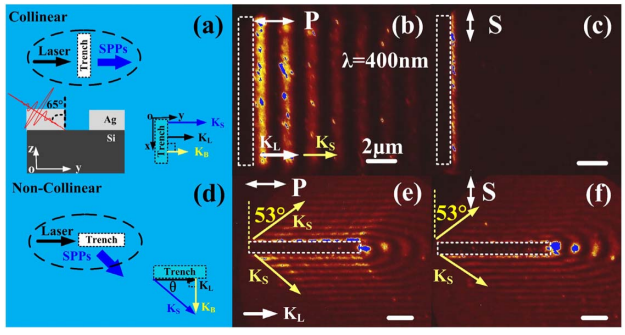

Fig. 1. Schematic of the experimental setup of the (a) collinear mode and (d) noncollinear mode for single-beam excitation. The femtosecond laser pulse illuminates the sample along the *y*-axis direction at an incidence angle 65° with respect to the surface normal of the silver film. The relation of wave vectors of the laser in-plane (k_L), SPP (k_S), and interference pattern (k_B) are displayed in (a) and (d), respectively. θ represents the direction of SPP propagation as shown in the inset of (d). PEEM images of the rectangular 10 μm × 1 μm trench structure after excitation are from the (b) *p*-polarized and (c) *s*-polarized under the collinear mode while from (e) *p*-polarized and (f) *s*-polarized under the noncollinear mode. The white dotted rectangles in (b), (c), (e), and (f) mark the trench.

balance the monochromaticity of an SPP pulse [23] and the intensity of nonlinear photoemission signals, the laser pulse with a pulse duration of 130 fs (narrow spectrum) aimed to illuminate the sample along the direction of the y axis at an incidence angle of 65° with respect to the surface normal of the sample [see inset in Fig. 1(a)], thereby generating an SPP from the trench structure. Moreover, the relation of wave vectors of the laser in-plane (k_L), SPP (k_S), and interference pattern (k_B), which satisfies Snell's law of refraction [24,25], is depicted in Figs. 1(a) and 1(d), respectively. Here, θ is the angle between k_L and k_S and represents the direction of SPP propagation, as shown in the inset of Figs. 1(a) and 1(d).

We recorded the multiphoton photoemission from a superposition of SPP and laser field using a photoemission electron microscope (Focus GmbH; see Methods). Figure 1(b) displays the PEEM image following irradiation with p-polarized femtosecond pulses ($\lambda = 400$ nm, second-harmonic generation from the femtosecond oscillator) of the collinear mode on the 10 μm × 1 μm trench structure milled into approximately 100 nm thick silver thin films by focused ion beam (FIB). A clear interference pattern induced by the incident femtosecond laser and the laser-induced SPP could be seen parallel to the trench. In the experiment, due to the 65° laser light incidence angle (as determined by the PEEM illumination configuration) with respect to the surface normal of the sample, two photon photoemission (2PP) signals ($\lambda = 400$ nm) could be seen being dominated by the out-of-plane component of the total polarization field, with negligible contribution from the in-plane component [6], i.e., the interference patterns are dominated by the out-of-plane field component of SPP and the laser light. Thus, the fringe in Fig. 1(b) reflects the information of the out-of-plane component of the field of SPP. Figure 1(c) displays the PEEM image with an s-polarized laser beam. Nevertheless, no interference pattern is observed in the PEEM image and the photoemission (PE) signal is localized in the edges of the trench when illuminating the trench with an s-polarized laser pulse. This result could be attributed to (i) the s-polarized light that does not couple efficiently to the SPP when the electric field of the incident light is parallel to the edge of the trench and (ii) both the orthogonal s-polarized light and SPP fields, which do not interfere due to the SPP being a transverse magnetic wave, i.e., there is no electric field component in the x direction (that is orthogonal to the propagation plane of SPP). An important hint from the measurement in Fig. 1(c) depicts that we might not be able to capture the in-plane field component of SPP using TR-PEEM when the probe light is s-polarized in the collinear mode. We confirmed this inference by the pump-probe experiment in the collinear excitation mode of the SPP (not shown in this work).

Figures 1(e) and 1(f) show the PEEM images of the same trench under the irradiation of p- and s-polarized beams of the noncollinear mode. Unlike the case of the collinear mode, the interference patterns are wing-shaped symmetrically on both sides of the trench, and obviously, the interference pattern had a sharp sloping boundary (shown by the yellow arrows). The boundary angle with respect to the normal of the trench was measured at approximately 53°, which was consistent with the direction of SPP propagation. The results intuitively show that such a sharply sloping boundary corresponds to the actual direction of SPP propagation, as we have proved using a 2D-wave simulation in our recent report [26]. Moreover, the interference fringe spacing Δl of the noncollinear mode [Figs. 1(e) and 1(f)] is subtle, at about 540 nm and supported by the simulation, and is far smaller than that of the collinear mode interference fringe with Δl being approximately 1.7 μm, as depicted in Fig. 1(b). More importantly, both the s- and p-polarized excitation lights are able to induce a moderate intensity of SPP in the noncollinear excitation of the trench, even though the SPP induced by s-polarized light excitation exhibits a weak SPP field. Thus, the noncollinear excitation of the trench offers possibility not only for capture of the out-of-plane components but also of the in-plane component of the SPP's electric field.

As principle proof of our new approach of disclosing TSAM of SPP through independent capture of the instantaneous phase information of out-of-plane and in-plane components of SPP near-fields, an experimental configuration for the capture of both components of SPP near-field is displayed in Fig. 2, considering the noncollinear mode. The femtosecond laser pulse is split into a pump-probe pulse pair; the timing of each could be independently controlled by a Mach–Zehnder interferometer setup, where the s- and p-polarization direction could be obtained by rotating a half-wave plate. To avoid entanglement of interference patterns in the PEEM image, especially for the static pattern induced by the pump laser and the laser-induced SPP and, simultaneously, to obtain the purely dynamic information of the SPP propagation, we separated the probe spatially and offset it temporarily from the pump in the TR-PEEM schemes, thereby enabling the time-resolved imaging of the SPP that was launched away from the coupling trench structure, as illustrated in Fig. 2.

It is known that the propagation distance of the SPPs is limited in several micrometers when the wavelength of excitation light is 400 nm, as shown in Fig. 1, which is because the imaginary part of the propagation wave vector for the Ag/vacuum interface, is large [27]. To ensure capturing a clear SPP propagation signal in the region away from the trench, we used

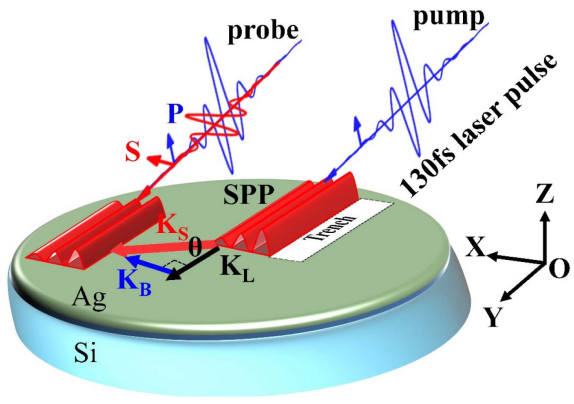

Fig. 2. Schematic illustrations of the spatially separated pump-probe experiment of the noncollinear mode. In the pump-probe schemes, the probe is spatially and temporally offset from the pump, affording time-resolved imaging of the SPP launched away from the coupling trench structure.

a 750 nm femtosecond laser pulse as the pumping source. Theoretically, the SPP excited by a 750 nm light would have a propagation distance on the silver film of about 250 μm [27]. Our measurement shows that the SPP propagation distance in Ag film is at least 235 μm (not shown in this work), which is enough to support our experiment. Figure 3 shows the PEEM images of the spatially separated pump-probe experiment of the noncollinear mode at the 20 μm × 1 μm trench structure. As demonstrated in our and other groups' previous work, a directional (efficient) excitation of the SPP along one side of the trench structure can be realized by adjusting the polarization direction of the incident light [25,26]. Therefore, in the time-resolved experiment of the noncollinear mode, the pump pulse with a polarization angle of 40° could be used to directionally excite the SPP, as shown in the insert in Fig. 3(a); eventually, the *p*- or *s*-polarized probe pulse would interrogate the SPP at a remote point.

Figure 3(a) displays the PEEM image with a pump-only 750 nm laser pulse. The angle of the propagation direction of the SPP with respect to the *y* axis is about 27°, which is consistent with the moiré pattern calculation [25]. Here, a damped ring-like interference pattern is observed to originate from the end of the trench. Figure 3(b) displays the PEEM image recorded with the probe laser only in a region 80 μm away from the trench on the flat silver film, while Fig. 3(c) displays the PEEM image following excitation with spatially separated femtosecond pulse pairs. We used the pump pulse with a

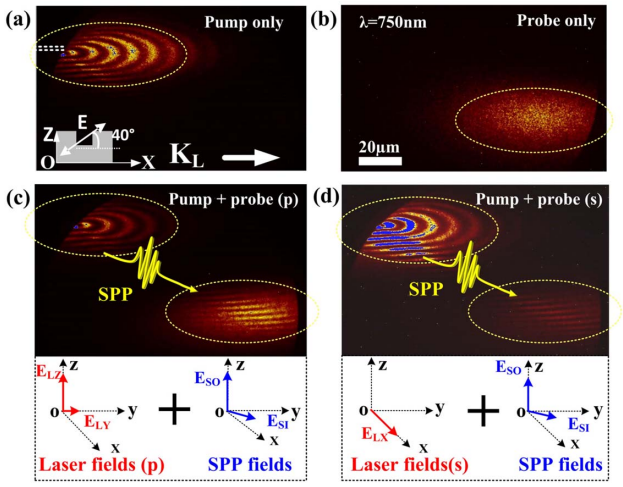

Fig. 3. PEEM images of the spatially separated pump-probe experiment of the noncollinear mode at 20 μm × 1 μm trench structure. The pump pulse with a polarization angle of 40° off the sample surface as indicated in insert of (a) is used efficiently to excite the SPP, and the *p*- or *s*-polarized probe pulse interrogates the SPP at a remote point. PEEM image with (a) pump-only and (b) probe-only from *p*-polarized 750 nm femtosecond laser. PEEM image obtained with a pump of 40°-polarized laser pulses and probe of (c) *p*-polarized pulses and (d) *s*-polarized pulses, respectively. The interference pattern by superposition of the laser and SPP electric field in the probe region can be seen in the inset of (c) and (d). White dashed rectangle is used to mark the location of the trench in (a), and yellow dashed ovals indicate the approximate positions of the spatially separated pump and probe beams. Zero delay is defined as the delays in which SPP of the pump launching and probe pulses are overlapped in time.

polarization angle of 40° off the sample surface, as indicated in by the insert in Fig. 3(a), to efficiently excite the SPP, which was followed by the *p*-polarized probe pulse interrogating the SPP at a remote point. The interference patterns induced by the probe pulse and the SPP wave packet are clearly observable in Fig. 3(c), which directly proves that the SPP and probe light demonstrated excellent coherence with each other. Interference patterns obtained from the interference of the *p*-polarized probe light with the SPP's electric field, along with the vectors diagram of the laser field and the SPP field, are shown at the bottom in Fig. 3(c). Recall from our discussion concerning Fig. 1(b) that the three photons photoemission (3PP) signal is dominated by the out-of-plane component of the total polarization field, with negligible contribution from the in-plane component [6], i.e., the interference patterns in Fig. 3(c) are dominated by the out-of-plane field component of SPP and the laser light, thus reflecting the spatiotemporal information of the out-of-plane component of the field of SPP. Logically, this demonstrates that the spatiotemporal information of the out-plane component of the field of SPP has been captured from the noncollinear mode using a *p*-polarized probe light. Figure 3(d) displays the PEEM image of the same delay time but is recorded with an *s*-polarized probe pulse. It is found that the photoemission intensity induced by the in-plane field is far weaker than that induced by the out-of-plane field. Moreover, the *s*-polarized probe laser field exists only in the plane of the sample. Observable interference patterns in the probe region of Fig. 3(d) result from the superposition of the in-plane field component of SPP and the laser light; the corresponding vector diagram of the laser field and the SPP field is given at the bottom in Fig. 3(d). This implies that the spatiotemporal information of the in-plane component of the field of SPP has likewise been captured in the noncollinear mode. The results show that the spatiotemporal information of the in-plane and out-of-plane components of the SPP near-field can be, respectively, captured from the noncollinear mode by time-resolved PEEM. The method may be used to reconstruct a 3D SPP spatiotemporal field.

Figure 4(a) describes the schematic of the experimental configuration, and the integrated photoemission signal over the *y* direction of the same SPP pulses in two arbitrary time domains and spaces (defined as regions of interest, ROIs 1 and 2, respectively, as indicated by the dotted line rectangles in the probe regions in the left panel). To ensure the capture of dynamic information of the same SPP pulses, during the experiment, the pump light is kept unchanged, and the position of the probe light and the delay time of the pump-probe pulse are adjusted. The intensity profile is obtained by subtracting the PE signal background extracted from the probe laser irradiated region. It is found that the fringe shift of the interference patterns with *s*- and *p*-polarized probe pulses is always $\Delta S/4$ (ΔS corresponds to the period of the interference fringes induced by the *s*- or *p*-polarized probe and with a value of 1.8 μm in PEEM image).

Insights into the origin of the fringe shift difference between the in-plane and out-of-plane electric field reveal that interference patterns are obtained by a classic wave simulation and FDTD simulation. For the wave simulation, the analytic

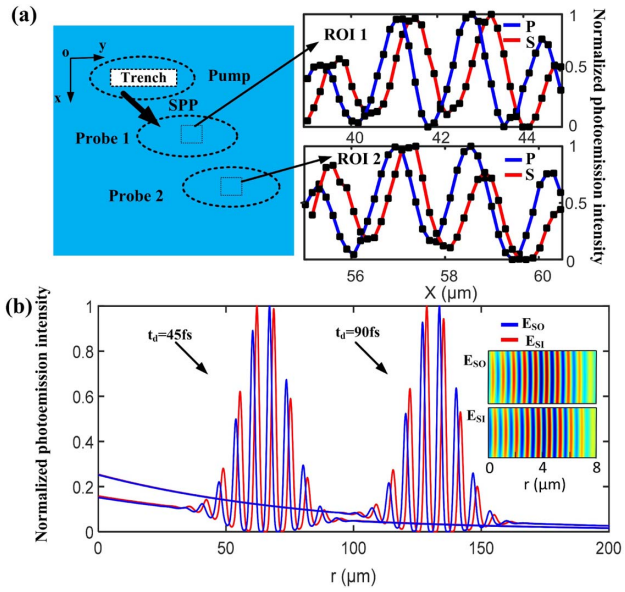

Fig. 4. (a) Schematic of experimental configuration and integrating the photoemission signal (PE) of the PEEM image over the x direction from the different regions of interest (ROIs). ROIs 1 and 2 correspond to the dashed rectangles in probe regions in the left panel. The cross-sectional profiles of the interference patterns in the probe regions obtained by subtracting the PE signal background extracted from the laser irradiated region are shown in the two right panels. (b) The intensity of the interference signals for the delays $t_d = 45$ and 90 fs simulated using a classical wave model. Meanwhile, FDTD calculation shows that the spatial distribution of out-of-plane and in-plane electric field components of the same SPP at the same time is always $\pi/2$ out of phase as shown in the inset of (b).

expression for the intensity of the interference pattern I_B in a 3PP-PEEM experiment at a distance r (the distance of SPP propagation) from the excitation edge is similar to [28,29],

$$I_B(r, t_d) = \int_{-\infty}^{+\infty} [E_L(r, t - t_d) + E_S(r, t)]^6 \mathrm{d}t, \quad (1)$$

where the incidence laser field is described with a Gaussian envelope,

$$E_L(r, t - t_d) = \mp E_0 \cdot \sin[k_L r - \omega_0 (t - t_d)] \cdot \exp\left[-\frac{1}{2}\left(\frac{r - c_L(t - t_d)}{c_L \tau}\right)^2\right]. \quad (2)$$

It is well known from the Jones matrix of the polarized light field that rotating the half-wave plate is not shifting the wavefront of the probe light. Here, we defined EL as positive for the 90° (p-polarized) and 0° (s-polarized) polarization angle of probe pulse and EL negative for the 180° (s-polarized) polarization angle of the probe pulse. Moreover, the imaginary longitudinal electric field of SPP generates the rotation of the electric field vector within the propagation plane corresponding to a $\pi/2$-phase difference between the E_{SO} (out-of-plane) and E_{SI} (in-plane) field components [1,2]; thus, the fields of E_{SO} and E_{SI} of SPP are described using the following expressions (for the sake of simplicity, the collinear excitation mode is simulated, which also supports our experimental results):

$$E_{SO}(r, t) = A_0 E_0 \cdot \sin(k_S r - \omega_0 t - \sigma) \cdot \exp\left[-\frac{1}{2}\left(\frac{r - v_g t}{v_g \tau}\right)^2\right] \cdot \exp\left(\frac{r}{L_S}\right), \quad (3)$$

$$E_{SI}(r, t) = A_1 E_0 \cdot \sin\left(k_S r - \omega_0 t - \sigma + \frac{\pi}{2}\right) \cdot \exp\left[-\frac{1}{2}\left(\frac{r - v_g t}{v_g \tau}\right)^2\right] \cdot \exp\left(\frac{r}{L_S}\right), \quad (4)$$

where

$$k_S = \mathrm{Re}\left[\frac{\omega_0}{c}\sqrt{\frac{\varepsilon(\omega_0)_m}{\varepsilon(\omega_0)_m + 1}}\right], \quad (5)$$

$$k_L = k_0 \cdot \sin 65°, \quad (6)$$

in which $\varepsilon(\omega_0)_m$ is the permittivity of silver, $c_L = \frac{c}{\sin\alpha}$ is the surface projected vacuum speed of light, and τ and ω_0 are the laser's pulse duration and frequency. The amplitude ratios A_0 and A_1 and the phase shift σ are between the excitation laser pulse and the SPP, depending on the excitation wavelength and the thickness of the film [30]. Consequently, when the wavelength of the laser pulse is 750 nm, the group velocity of the SPPs v_g is approximately $0.93c$, as reported in Ref. [31]. Additionally, L_S is the theory propagation distance of SPPs in the silver film surface for the 750 nm laser pulse. It is also worth mentioning that we adopted the dielectric permittivity of silver as defined by Johnson and Christy [22]. Furthermore, to obtain a pure and clear dynamic information of the SPP propagation, we used a probe pulse of $\tau = 10$ fs for the simulation and only considered the interference signal of the SPP (pump pulse excitation) and the probe pulse.

Figure 4(b) displays the interference signals for the delay times $t_d = 45$ and 90 fs simulated using the classical wave model. Interference shifts between the superposition of E_{SO} with the p-polarized probe light and E_{SI} with the s-polarized probe light demonstrated that the fringe shift of the interference patterns is always $\Delta S'/4$ ($\Delta S'$ corresponds to the period of the interference fringes induced by the s- or p-polarized probe), consistent with that obtained in the experimental result in Fig. 4(a). It is known from Fig. 4(b) that the fringe shift of the interference patterns of $\Delta S'/4$ was the result of the $\pi/2$ phase difference between the in-plane and out-of-plane components of the SPP field. Thus, we can deduce that the fringe shift of the interference patterns of $\Delta S/4$ we obtained in Fig. 4(a) could be attributed to a $\pi/2$ phase difference between the in-plane and out-of-plane electric field components of SPP. Moreover, FDTD calculations revealed the spatial distribution of the out-of-plane and in-plane electric field components of the same SPP, which simultaneously correspond to a $\pi/2$ out of phase, as shown in the inset in Fig. 4(b). Therefore, the $\pi/2$ phase difference based on the measurement in Fig. 4(a) originates from the inherent property of the SPP electric field in the space–time evolution and discloses the basic elements consisting of the TSAM of the SPP. Furthermore, the results presented in Fig. 4(a) undoubtedly provide direct evidence of SPP exhibiting an elliptically polarized electric field in the

propagation plane and characterized by TSAM [1]. It should be mentioned that the amplitude difference of out-of-plane and in-plane components cannot be quantitatively obtained due to a different ability of emitting photoelectron between *p*- and *s*-polarized incident light fields or out-of-plane and in-plane components of the same field intensity. Essentially, it is a reliable suggestion for TSAM of SPP to be verified by independently capturing its instantaneous phase information of out-of-plane and in-plane near-fields. Despite the existence of the interference of in-plane components along the *y* direction under *p*-polarization conditions, the contribution of SPP in-plane components to multiphoton photoemission can be considered negligible. In such a case, the accurate capture of out-of-plane component phase information can be ensured.

4. CONCLUSIONS

In summary, we performed an experimental demonstration pertaining to the separation of the out-of-plane and in-plane components of the SPP near-fields by spatiotemporal imaging via utilization of *p*- and *s*-polarized probe light, respectively, under the noncollinear mode. Our experimental results essentially showed that instantaneous out-of-plane and in-plane components of the SPP near-fields are always $\pi/2$ out of phase; here, we supported the resulting time-resolved PEEM images with a classical wave model and FDTD simulations. The results provided direct evidence that SPP exhibits an elliptically polarized electric field in the propagation plane and is characterized by TSAM. Moreover, this study showcased the ability of the PEEM technology to conduct independent, spatiotemporal imaging of the in- and out-of-plane components of SPP near-fields, which may pave the way toward further independent explorations on the potential contribution of the in- and out-of-plane components of SPP near-fields in the direction of photoemission. We also expect it to provide a scheme for the reconstruction of the 3D SPP spatiotemporal field.

Funding. National Natural Science Foundation of China (91850109, 61775021, 11474040); Education Department of Jilin Province (JJKH20181104KJ, JJKH20190549KJ, JJKH20190555KJ); "111" Project of China (D17017); Changchun University of Science and Technology (XQNJJ-2018-02).

Acknowledgment. Authors thank Key Laboratory for Cross-Scale Micro and Nano Manufacturing of the Ministry of Education, Changchun University of Science and Technology.

Disclosures. The authors declare no conflicts of interest.

REFERENCES

1. K. Y. Bliokh and F. Nori, "Transverse spin of a surface polariton," Phys. Rev. A **85**, 061801 (2012).
2. K. Y. Bliokh, A. Y. Bekshaev, and F. Nori, "Extraordinary momentum and spin in evanescent waves," Nat. Commun. **5**, 3300 (2014).
3. T. V. Mechelen and Z. Jacob, "Universal spin-momentum locking of evanescent waves," Optica **3**, 118–126 (2016).
4. K. Y. Bliokh, D. Smirnova, and F. Nori, "Quantum spin Hall effect of light," Science **348**, 1448–1451 (2015).
5. Y. Dai and H. Petek, "Plasmonic spin-Hall effect in surface plasmon polariton focusing," ACS Photon. **6**, 2005–2013 (2019).
6. Y. Dai, M. Dąbrowski, V. A. Apkarian, and H. Petek, "Ultrafast microscopy of spin-momentum-locked surface plasmon polaritons," ACS Nano **12**, 6588–6596 (2018).
7. A. Hayat, J. B. Mueller, and F. Capasso, "Lateral chirality-sorting optical forces," Proc. Natl. Acad. Sci. USA **112**, 13190–13194 (2015).
8. D. O'Connor, P. Ginzburg, F. J. Rodríguez-Fortuño, G. A. Wurtz, and A. V. Zayats, "Spin-orbit coupling in surface plasmon scattering by nanostructures," Nat. Commun. **5**, 5327 (2014).
9. K. Imaeda, S. Hasegawa, and K. Imura, "Static and dynamic near-field measurements of high-order plasmon modes induced in a gold triangular nanoplate," J. Phys. Chem. Lett. **9**, 4075–4081 (2018).
10. Y. Gorodetski, T. Chervy, S. Wang, J. A. Hutchison, A. Drezet, C. Genet, and T. W. Ebbesen, "Tracking surface plasmon pulses using ultrafast leakage imaging," Optica **3**, 48–53 (2016).
11. B. Wild, L. Cao, Y. Sun, B. P. Khanal, E. R. Zubarev, S. K. Gray, N. F. Scherer, and M. Pelton, "Propagation lengths and group velocities of plasmons in chemically synthesized gold and silver nanowires," ACS Nano **6**, 472–482 (2012).
12. B. Le Feber, N. Rotenberg, D. Van Oosten, and L. Kuipers, "Modal symmetries at the nanoscale: a route toward a complete vectorial near-field mapping," Opt. Lett. **39**, 2802–2805 (2014).
13. B. N. Tugchin, N. Janunts, A. E. Klein, M. Steinert, S. Fasold, S. Diziain, M. Sison, E. B. Kley, A. Tünnermann, and T. Pertsch, "Plasmonic tip based on excitation of radially polarized conical surface plasmon polariton for detecting longitudinal and transversal fields," ACS Photon. **2**, 1468–1475 (2015).
14. J. Yang, Q. Sun, K. Ueno, X. Shi, T. Oshikiri, H. Misawa, and Q. Gong, "Manipulation of the dephasing time by strong coupling between localized and propagating surface plasmon modes," Nat. Commun. **9**, 4858 (2018).
15. Y. Gong, A. G. Joly, D. Hu, P. Z. El-Khoury, and W. P. Hess, "Ultrafast imaging of surface plasmons propagating on a gold surface," Nano Lett. **15**, 3472–3478 (2015).
16. A. Kubo, N. Pontius, and H. Petek, "Femtosecond microscopy of surface plasmon polariton wave packet evolution at the silver/vacuum interface," Nano Lett. **7**, 470–475 (2007).
17. P. Kahl, D. Podbiel, C. Schneider, A. Makris, S. Sindermann, C. Witt, M. Horn-von Hoegen, M. Aeschlimann, and F. J. M. zu Heringdorf, "Direct observation of surface plasmon polariton propagation and interference by time-resolved imaging in normal-incidence two photon photoemission microscopy," Plasmonics **13**, 239–246 (2018).
18. P. Kahl, S. Wall, C. Witt, C. Schneider, D. Bayer, A. Fischer, P. Melchior, M. Horn-von Hoegen, M. Aeschlimann, and F. J. M. zu Heringdorf, "Normal-incidence photoemission electron microscopy (NI-PEEM) for imaging surface plasmon polaritons," Plasmonics **9**, 1401–1407 (2014).
19. R. C. Word and R. Könenkamp, "Photonic and plasmonic surface field distributions characterized with normal-and oblique-incidence multi-photon PEEM," Ultramicroscopy **183**, 43–48 (2017).
20. D. Podbiel, P. Kahl, A. Makris, B. Frank, S. Sindermann, T. J. Davis, M. Horn-von Hoegen, H. Giessen, and F. J. Meyer zu Heringdorf, "Imaging the nonlinear plasmoemission dynamics of electrons from strong plasmonic fields," Nano Lett. **17**, 6569–6574 (2017).
21. B. Ji, J. Qin, H. Tao, Z. Hao, and J. Lin, "Subwavelength imaging and control of ultrafast optical near-field under resonant-and off-resonant excitation of bowtie nanostructures," New J. Phys. **18**, 093046 (2016).
22. P. B. Johnson and R. W. Christy, "Optical constants of the noble metals," Phys. Rev. B **6**, 4370–4379 (1972).
23. T. Wang, G. Comtet, E. Le Moal, G. Dujardin, A. Drezet, S. Huant, and E. Boer-Duchemin, "Temporal coherence of propagating surface plasmons," Opt. Lett. **39**, 6679–6682 (2014).
24. M. Dąbrowski, Y. Dai, and H. Petek, "Ultrafast microscopy: imaging light with photoelectrons on the nano-femto scale," J. Phys. Chem. Lett. **8**, 4446–4455 (2017).
25. Y. Gong, A. G. Joly, P. Z. El-Khoury, and W. P. Hess, "Polarization-directed surface plasmon polariton launching," J. Phys. Chem. Lett. **8**, 49–54 (2016).

26. Y. Qin, X. Song, B. Ji, Y. Xu, and J. Lin, "Demonstrating a two-dimensional-tunable surface plasmon polariton dispersion element using photoemission electron microscopy," Opt. Lett. **44**, 2935–2938 (2019).
27. W. L. Barnes, A. Dereux, and T. W. Ebbesen, "Surface plasmon subwavelength optics," Nature **424**, 824–830 (2003).
28. C. Lemke, T. Leißner, A. Klick, J. Fiutowski, J. W. Radke, M. Thomaschewski, J. Kjelstrup-Hansen, H. G. Rubahn, and M. Bauer, "The complex dispersion relation of surface plasmon polaritons at gold/para-hexaphenylene interfaces," Appl. Phys. B **116**, 585–591 (2014).
29. L. Zhang, A. Kubo, L. Wang, H. Petek, and T. Seideman, "Imaging of surface plasmon polariton fields excited at a nanometer-scale slit," Phys. Rev. B **84**, 245442 (2011).
30. A. Klick, S. de la Cruz, C. Lemke, M. Großmann, H. Beyer, J. Fiutowski, H.-G. Rubahn, E. R. Méndez, and M. Bauer, "Amplitude and phase of surface plasmon polaritons excited at a step edge," Appl. Phys. B **122**, 79 (2016).
31. V. V. Temnov, U. Woggon, J. Dintinger, E. Devaux, and T. W. Ebbesen, "Surface plasmon interferometry: measuring group velocity of surface plasmons," Opt. Lett. **32**, 1235–1237 (2007).